JOURNAL OF GEOPHYSICAL RESEARCH: ATMOSPHERES, VOL. 118, 846–858, doi:10.1029/2012JD018515, 2013

Validation of a radiosonde-based cloud layer detection method against a ground-based remote sensing method at multiple ARM sites

Jinqiang Zhang,[1,2] Zhanqing Li,[1,2,3] Hongbin Chen,[1] and Maureen Cribb[2]

Received 19 July 2012; revised 18 December 2012; accepted 5 October 2012; published 31 January 2013.

[1] Cloud vertical structure is a key quantity in meteorological and climate studies, but it is also among the most difficult quantities to observe. In this study, we develop a long-term (10 years) radiosonde-based cloud profile product for the U.S. Department of Energy's Atmospheric Radiation Measurement (ARM) program Southern Great Plains (SGP), Tropical Western Pacific (TWP), and North Slope of Alaska (NSA) sites and a shorter-term product for the ARM Mobile Facility (AMF) deployed in Shouxian, Anhui Province, China (AMF-China). The AMF-China site was in operation from 14 May to 28 December 2008; the ARM sites have been collecting data for over 15 years. The Active Remote Sensing of Cloud (ARSCL) value-added product (VAP), which combines data from the 95-GHz W-band ARM Cloud Radar (WACR) and/or the 35-GHz Millimeter Microwave Cloud Radar (MMCR), is used in this study to validate the radiosonde-based cloud layer retrieval method. The performance of the radiosonde-based cloud layer retrieval method applied to data from different climate regimes is evaluated. Overall, cloud layers derived from the ARSCL VAP and radiosonde data agree very well at the SGP and AMF-China sites. At the TWP and NSA sites, the radiosonde tends to detect more cloud layers in the upper troposphere.

Citation: Zhang, J., Z. Li, H. Chen, and M. Cribb (2013), Validation of a radiosonde-based cloud layer detection method against a ground-based remote sensing method at multiple ARM sites, *J. Geophys. Res. Atmos.*, *118*, 846–858, doi:10.1029/2012JD018515.

1. Introduction

[2] Cloud vertical structure and the distribution of multilayered clouds within the atmosphere affect atmospheric dynamics, thermodynamics, and the hydrological cycle, as well as the radiation budget at the surface and within the atmosphere [*Chahine et al.*, 2006; *Li et al.*, 2005]. Radiosondes can penetrate cloud layers thus providing in situ measurements of temperature and humidity that may convey information about clouds. To take advantage of the global long-term set of radiosonde data, methods have been developed to determine the locations and boundaries of cloud layers from radiosonde data [*Arabey*, 1975; *Air Weather Service*, 1979; *Dolgin*, 1983]. *Poore et al.* [1995] used rawinsonde observations to determine the boundaries of cloud layers by testing dew point temperature depressions below some threshold values. *Wang and Rossow* [1995] (hereafter WR95) used relative humidity (RH) profiles to obtain cloud vertical structure with a transformation of RH to that with respect to ice at levels where the temperature is below 0°C. *Chernykh and Eskridge* [1996] developed a cloud detection method based on the second-order derivatives of temperature and RH with respect to height. Cloud boundaries are defined if at least one of the two second-order derivatives is 0. Using radiosonde data, many studies have developed and analyzed cloud vertical structure [e.g., *Wang et al.*, 1999, 2000; *Chernykh et al.*, 2000; *Minnis et al.*, 2005], but few have been validated due to a lack of trustworthy and/or independent products [e.g., *Wang et al.*, 1999; *Naud et al.*, 2003]. Another limitation stems from the fact that the vast majority of radiosonde data are only available at a highly limited number of standard and significant vertical levels mandated by the World Meteorological Organization, which can severely hinder our ability to obtain a true picture of cloud vertical distribution.

[3] Modifying the method of WR95, we used radiosonde data obtained from the Atmospheric Radiation Measurement (ARM) mobile facility (AMF) campaign in China to analyze cloud distributions at a site in southeastern China [*Zhang et al.*, 2010]. The deployment of the AMF in China (AMF-China) was part of a major U.S.–China joint experiment called the East Asian Studies of Tropospheric Aerosols and their Impact on Regional Climate (EAST-AIRc) [*Li et al.*, 2010, 2011a]. While W-Band (95 GHz) cloud radar (WACR) imagery

[1]Key Laboratory of the Middle Atmosphere and Global Environmental Observation, Institute of Atmospheric Physics, Chinese Academy of Sciences, Beijing, China.
[2]Department of Atmospheric and Oceanic Science and Earth System Science Interdisciplinary Center, University of Maryland, College Park, Maryland, USA.
[3]State Key Laboratory of Earth Surface Processes and Resource Ecology, GCESS, Beijing Normal University, 100875, Beijing, China.

Corresponding author: Z. Li, State Key Laboratory of Earth Surface Processes and Resource Ecology, GCESS, Beijing Normal University, Beijing, China. (zhanqingli@msn.com)

2169-897X/13/2012JD018515

were useful in developing the radiosonde-based algorithm [*Zhang et al*., 2010], a rigorous validation was not carried out at the time because the official ARM cloud value-added product (VAP) based on multiple sensors was not released until recently.

[4] At the Central Facility in the Southern Great Plains (SGP), the first ARM field measurement site near Lamont, Oklahoma, the cloud VAP has been generated since 1996 by applying the algorithm of *Clothiaux et al*. [2000] to data collected from a suite of remote sensing instruments. Given the long-term nature of the SGP VAP product, many studies have been carried out concerning clouds. *Dong et al*. [2005, 2006], for example, found that cloud-layer altitudes and physical thicknesses were higher and greater in summer than in winter, and they determined that annual averages of total and single-layered low-, middle-, and high-cloud fractions were 0.49, 0.11, 0.03, and 0.17, respectively, between January 1997 and December 2002 over the SGP site. *Xi et al*. [2010] extended the period to December 2006 and found that the mean cloud fraction was 46.9% and varied seasonally from a summer minimum of 39.8% to a maximum of 54.6% during the winter. *Kollias et al*. [2007] found that cirrus was the most frequently observed cloud type over the SGP site and that there was a strong seasonal variability in cloud-base heights and relatively constant cloud fractions. *Mace and Benson* [2008] confirmed that the vertical profile of cloud occurrence was dominated by clouds in the upper troposphere and in the boundary layer, consistent with a global satellite cloud product [*Chang and Li*, 2005a] generated from an algorithm that takes advantage of multiple MODIS channels [*Chang and Li*, 2005b]. By examining the long-term impact of aerosols on the vertical development of clouds at the SGP site, *Li et al*. [2011b] and *Niu and Li* [2012] found that the cloud-top height and thickness for mixed-phase clouds with warm, low bases increased with aerosol concentration measured near the ground; no change was seen in cloud-top height with aerosol concentration for clouds with cool bases. The effect depends on cloud profile and meteorological variables [*Fan et al*., 2009, 2012].

[5] The second ARM climate research facility was established in the Tropical Western Pacific (TWP) region, which plays a large role in the interannual variability observed in the global climate system. Data from the Manus facility on Los Negros Island in Manus, Papua New Guinea, which was established in 1996 as one facility in the TWP, is used in this study. The North Slope of Alaska (NSA) site provides information about cloud and radiative processes at high latitudes. This site has become a focal point for atmospheric and ecological research activities on the North Slope. Data from the principal instrumented facility installed near Barrow in 1997 is used here. Many studies focused on cloud properties were also conducted at the TWP [e.g., *Jakob et al*., 2005; *Pavolonis et al*., 2005; *Mather et al*., 2007] and NSA sites [e.g., *Dong and Mace*, 2003; *Xie et al*., 2006; *Marchand et al*., 2007; *Zhao and Wang*, 2010].

[6] Clouds are an extremely important aspect of the Earth's climate system [*Lazarus et al*., 2000; *Zhang and Klein*, 2010]. A popular use of these observations is to evaluate cloud parameterizations in climate models [*Qian et al*., 2012]. Unfortunately, detailed observations of clouds are not available globally. Instead, we are limited to extensive surface sites such as those developed by the ARM project. Some progress has been made in recent years with active sensing satellites such as CloudSat [e.g., *Stephens et al*., 2002; *Mace et al*., 2009; *Oreopoulos and Norris*, 2011]; however, additional observations are desperately needed. Balloon soundings have been used in the past to obtain cloud information, but have been validated on only a few occasions. At the ARM SGP site, radiosondes have been launched four times a day since 1992, but this data has not been used to generate any cloud product. While this may be unnecessary at this site, given the high quality, good continuity and long duration of the cloud VAP product, it is useful to compare the VAP product against the radiosonde product for two reasons, which is where this paper fits in. First, the atmospheric profile data provided by the radiosonde conveys valuable and independent information on the presence of clouds that could help identify any deficiencies of the ground-based remote sensing product, and vice versa. Second, radiosonde data from around the world have been collected routinely for many decades, whereas only a handful of ARM-like stations have been established over the past decade, such as the Cloudnet in Europe [e.g., *Haeffelin et al*., 2005; *Illingworth et al*., 2007].

[7] The coexistence of ground-based remote sensing instruments at the ARM sites, in particular, cloud radars and radiosondes, presents a unique opportunity to evaluate cloud products derived from their measurements through intercomparisons in order to help identify their advantages and limitations, which is the primary objective of this study. In *Zhang et al*. [2010], an algorithm was developed to determine cloud layers from balloon soundings released at the AMF deployed in Shouxian, China. At that time, the VAP derived from radar data did not exist. This paper expands on the previous work by comparing the algorithm to ARSCL data acquired from the short-term AMF campaign in China and by expanding the technique to long-term data collected at the SGP, TWP, and NSA sites, which represent different climate regimes. Section 2 describes the cloud detection algorithms and data used in this study. Comparisons of the two cloud products collected at the AMF-China site and interpretation of the results are presented in section 3. Similar content for the SGP, TWP, and NSA sites is presented in section 4. Main conclusions are summarized in section 5.

2. Cloud Detection Algorithms and Data

2.1. Radiosonde-Based Method and Product

[8] The algorithm of *Zhang et al*. [2010] is modified from *Wang and Rossow* [1995]. It employs three height-resolving RH thresholds to determine cloud layers: minimum and maximum RH thresholds in cloud layers (min-RH and max-RH), and minimum RH thresholds within the distance of two contiguous layers (inter-RH). Before applying any test, RH was first transformed with respect to ice instead of liquid water for all levels with temperatures below 0°C. It was then examined to identify cloud layers in eight steps: (1) the base of the lowest moist layer was determined as the level where RH exceeded the min-RH corresponding to this level; (2) above the base of the moist layer, contiguous levels with RH over the corresponding min-RH were treated as the same layer; (3) the top of the moist layer was identified when RH decreased to that below the corresponding min-RH or RH was over the corresponding min-RH but the top of the profile was reached; (4) moist layers with bases lower than 120 m and thicknesses less than 400 m were discarded; (5) the moist layer was classified as a cloud layer if the

maximum RH within this layer was greater than the corresponding max-RH at the base of this moist layer; (6) the base of cloud layers was set to 280 m Above Ground Level (AGL) and cloud layers were discarded if their tops were lower than 280 m; (7) two contiguous layers were considered as a one-layer cloud if the distance between these two layers was less than 300 m or the minimum RH within this distance was more than the maximum inter-RH value within this distance; and (8) clouds were discarded if their thicknesses were less than 30.5 m for low clouds, and 61 m for middle/high clouds.

[9] We applied the method to generate cloud layer products from radiosonde data acquired during the AMF deployment in Shouxian, Anhui Province (32.56°N, 116.78°E, and 21 m above sea level) from May 14 to December 28, 2008 [*Zhang et al*., 2010], as well as to the ARM SGP routine radiosonde launches from 1 January 2001 to 1 December 2010. During the AMF-China campaign, Vaisala RS92-SGP radiosondes were launched four times a day without any major interruption; launch times were at 05:30, 11:30, 17:30 and 23:30 Coordinated Universal Time (UTC). Of all the launches, 813 of them reached altitudes greater than 10 km. At the SGP site, a minimum of four radiosonde launches are made daily; more frequent launches were made during intensive field campaigns, such as the Atmospheric Infrared Sounder Campaign [*Tobin et al*., 2006] and the Cloud Land Surface Interaction Campaign [*Miller*, 2008]. At the TWP and NSA sites, two radiosonde launches are generally made daily.

2.2. Ground-Based Cloud Detection Algorithm and Products

[10] Ground-based active remote sensors, such as the 35-GHz Millimeter Microwave Cloud Radar (MMCR) [*Moran et al*., 1998], are capable of detecting multiple cloud layers with high temporal and vertical resolutions so can provide detailed information about cloud layer overlap. The MMCR operates in four modes [*Clothiaux et al*., 1999] to provide continuous profiles of radar reflectivity by hydrometeors within its field of view, allowing for the determination of cloud layers. The laser ceilometer and the micropulse lidar (MPL) are sensitive to the second moment of the particle distribution; however, the MMCR is sensitive to the sixth moment so it can readily detect nonhydrometeors associated with insects and bits of vegetation. So the ceilometer and MPL can provide a more reliable estimate of cloud-base heights than can the MMCR. By combining observations from the cloud radar, the MPL, and the ceilometer, the ARSCL VAP was generated to detect cloud boundaries with the best possible accuracy [*Clothiaux et al*., 1999, 2000; *Kollias et al*., 2009].

[11] A Vaisala ceilometer and an MPL collected measurements during the entire duration of the AMF-China; the 95-GHz W-band ARM Cloud Radar (WACR) operated from 15 October to 15 December 2008 in China. The WACR VAP has a temporal resolution of five seconds and a vertical resolution of 45 m; up to ten cloud layers boundaries can be identified. At the SGP, TWP, and NSA sites, the MMCR was deployed from which the MMCR VAP product with a temporal resolution of ten seconds was derived [*Miller et al*., 2003]. The MMCR VAP data streams at the SGP site ended as of 4 January 2011 because the MMCR was taken out of service and replaced by an upgraded radar called the 'KAZR' (Ka-band ARM Zenith-pointing Radar) whose cloud product is currently under development. The ARSCL VAP generated from 1 January 2001 to 31 December 2010 at the SGP site, 7 March 2002 to 7 March 2011 at the TWP site, and 28 April 2002 to 23 March 2011 at the NSA site is used in this study. To differentiate the two somewhat different cloud VAP products, WVAP is used to refer to the product from China and ARSCL is used to refer to the product elsewhere.

3. Comparison of Cloud Layers Derived From Radiosonde Data and the WVAP Data in China

[12] When comparing the two cloud data sets, consideration must be taken of the differences caused by balloon drifting and the instantaneous nature of ground-based remote sensing measurements taken at a fixed site. Because of the movements of clouds, comparisons of cloud boundaries cannot be limited to an instantaneous moment, but must be made for a time range which is set to $\pm 1/2$ h in this study. Note that one radiosonde launch usually takes about 1.5 h to complete, but in the last half-hour, the balloon usually goes beyond the troposphere.

[13] In total, 297 individual cloud layers were derived from the 248 radiosonde launches from 15 October to 15 December 2008 when the WVAP is available. The vertical distribution of cloud layers obtained from the radiosonde and the WVAP during the above period is shown in Figure 1. Figure 1a is the contour plot of cloud distribution determined from the radiosonde. Figure 1b plots the time series of cloud profiles detected by the WVAP but only at the time of radiosonde launches. Figure 1c is the same as Figure 1b but for all available data samples. Cloud distributions from the radiosonde and the WVAP agree well. Although radiosondes are launched only four times a day, they can capture the gross features of cloud temporal variations and vertical distributions well, with reference to the WVAP product. However, there are obvious differences in detecting cloud layers near the surface, as seen in Figures 1a and 1b. Of the 248 radiosonde launches, no clouds with bases located below than 1 km were detected by both the radiosonde and the WVAP in 161 (64.9%) of the cases, while both methods detected such clouds in 25 (10.1%) of the cases. In 58 (23.4%) of the launches, the WVAP detected such clouds but the radiosonde did not; the radiosonde detected such clouds while the WVAP did not in 1.6% of the cases.

[14] Part of the discrepancies between the radiosonde and the WVAP results originate from different limits accepted for the lowest clouds. The ceilometer and MPL can provide a more reliable estimate of cloud-base height than can the cloud radar within the range of instrument detection. In the presence of precipitation below the cloud base, even cloud-base heights derived from the ceilometer and MPL are problematic [*Clothiaux et al*., 2000; *Nowak et al*., 2008]. The radiosonde cloud retrieval method based on RH also encounters difficulties in discriminating between cloud layers and moist layers near the surface because these layers may be associated with drizzle or rain. The lowest cloud-base height was set to 280 m in *Zhang et al*. [2010]. However, it is set to 136 m in the WVAP algorithm. To remove differences caused by this artificial threshold, the lowest cloud-base height is reduced from 280 m to 136 m in the

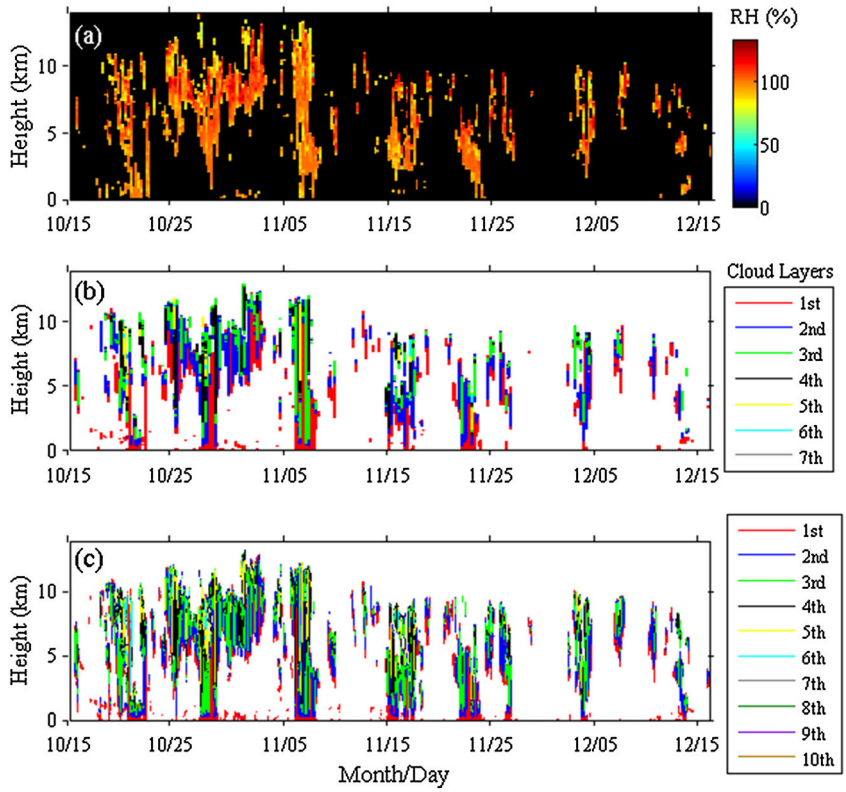

Figure 1. Cloud vertical distributions from (a) radiosonde measurements, (b) the WVAP during radiosonde launches only, and (c) all data from the WVAP. The RH within clear layers in Figure 1a are set to 0. Different colors in Figures 1b and 1c denote cloud boundaries for different cloud layers from the surface upward.

radiosonde results presented here. The restriction imposed in our previous analysis that discards cloud layers with bases lower than 120 m and thicknesses less than 400 m is lifted here. These changes result in the detection of more low-level cloud layers from the radiosonde although it is still much less than the number of cloud layers with bases less than 1 km generated by the WVAP.

[15] An example illustrating how the radiosonde misses near-surface cloud layers is given in Figure 2 for the radiosonde launch on 19 October 2008 at 05:27 UTC. Figure 2a shows the cloud mask from the WVAP during the 30 min after the radiosonde launched. Profiles of RH with respect to water and ice for atmospheric temperature above and below 0°C, respectively, are shown in Figure 2b. The gray

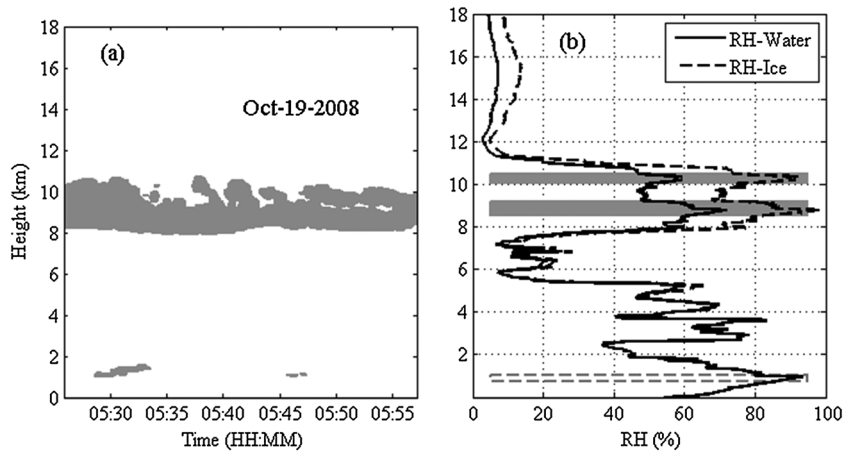

Figure 2. Comparison of cloud layers obtained from (a) WVAP and (b) radiosonde data. Radiosonde vertical profiles of RH with respect to water, RH with respect to ice when temperatures are less than 0°C, and cloud layer boundaries are shown by the solid black line, the dashed black line, and the area colored cyan, respectively; the rectangle outlined by a dashed gray line represents the additional cloud layer identified by the radiosonde after the retrieval method was revised.

shaded areas represent the locations of cloud layers from the radiosonde. Cloud layers between 8.5 km and 11 km were identified by both radiosonde and WVAP retrievals. However, thin layers near the surface were detected by the WVAP but were classified as clear by the radiosonde. The following two factors may explain why the radiosonde missed the low cloud layers. The first factor is associated with the short life time and small spatial coverage of the cloud layer, and the nature of radiosonde drift. In this case, it means that the radiosonde simply did not go through these particular cloud layers. The second factor is the time lag error of the radiosonde hygrometer. Given the sharp gradient of RH and thinness of the cloud layer, there is not enough time for the hygrometer to reach equilibrium. Because the RH increases from less than 60% at the surface to greater than 90% at 0.9 km (Figure 2b), we believe that a true cloud layer near surface was identified by the WVAP. A closer look at all the data reveals similar problems occurring in many other cases.

[16] From all cloud cases found during the AMF, a total of 2775 samples were identified as cloud layers near the surface by the WVAP (within $\pm 1/2$ h of the radiosonde launched time) but were not detected by the radiosonde. Figure 3 shows the frequency of occurrence of RH and maximum RH within these cloud layers; the two curves are similar. The bulk of the measurements of RH and maximum RH lie between 50 and 85% and any changes are chiefly caused by increases with height. We postulate that they correspond to a common scenario of drizzling low clouds. For these clouds, RH is high near the cloud base but evaporation of the drizzle causes a rapid decrease of RH toward the surface. Apparently, these clouds do not reach ground. As a result of this finding, we revised our algorithm by introducing a test requiring that the rate of RH change near the surface below 1 km be greater than 15%/km and that the maximum RH exceed 85%. Cloud layer thickness must still be greater than 30.5 m. After implementing this modification, the lowest cloud layer detected by the radiosonde is now shown as the rectangle outlined by the dashed gray line in Figure 2b. This change to the algorithm leads to a significant improvement in agreement with the WVAP for detecting near-surface clouds.

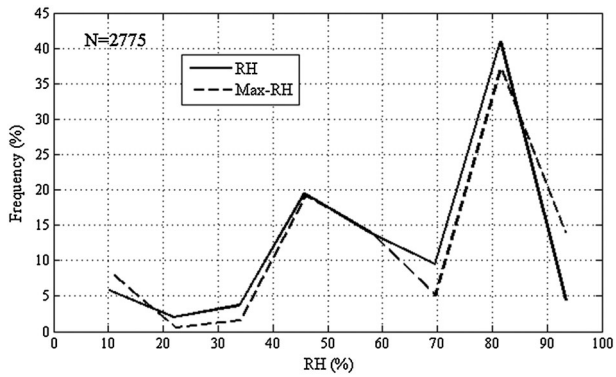

Figure 3. Frequency distributions of RH (solid line) and maximum RH (dashed line) within near-surface WVAP cloud layers missed by the radiosonde.

[17] Table 1 gives the total number and frequencies (in percentage) of four matching scenarios: (1) where both methods detected clouds, (2) where both did not, (3) where the WVAP detected a cloud layer but the radiosonde did not, and (4) where the radiosonde detected a cloud layer but the WVAP did not. In this comparison, cloud height is disregarded, which is addressed below. The two methods agree for the vast majority of cases with a success score of 92%. The comparison of cloud layers obtained from radiosonde measurements and the WVAP are further analyzed in Figure 4. Encouraging results are found when the number of cloud layers identified by the two methods is compared, as illustrated in Figure 4a, which shows the frequency distributions of the occurrence of clear layers, and single or multilayer clouds from all radiosonde and WVAP retrievals. The two sets of distributions are similar with the single layer of cloud as the most common cloud configuration. The WVAP detected more single-layer clouds than multilayer clouds compared to what the radiosonde detected, but the opposite is true for multilayer clouds. This can be partly explained by the difference in the observation interval. The data frequency of the WVAP is 5 s; however, the radiosonde completes one flight in over more than 90 min during which more cloud layers may be encountered.

[18] Figure 4b shows the frequency distributions of cloud-base height, cloud-top height, and cloud thickness for all cloud layers detected by the radiosonde and the WVAP. They all match fairly closely although some discrepancies arise at a more detailed level. The frequency distributions of cloud-base height at altitudes higher than 7 km and cloud-top height at altitudes higher than 10 km from the radiosonde are generally larger than those from the WVAP. This indicates that more high-level cloud layers were detected by the radiosonde than by the WVAP and that they were positioned higher in the upper troposphere. This may be explained by the following: (1) the uppermost layers might be missed by the WVAP due to the attenuation effect of thick lower-level clouds and fog on laser beams, and (2) the RH thresholds used for high altitudes in this study are smaller than those used in *Wang and Rossow* [1995], which results in the detection of more high cloud layers.

[19] The locations of cloud boundaries from individual radiosonde and WVAP observations are compared in Figures 5a and 5b. Colored dots represent different radiosonde drift distance (DD). Overall, both cloud-base heights and cloud-top heights derived from the two distinctly different approaches agree very well, as the vast majority of data points are along the 1:1 line; the correlation coefficients are 0.91 and 0.92, respectively. A close inspection of the outlier cases shows that those above the 1:1 line and below 1 km along the x axis correspond to low-level moist layers with large

Table 1. Comparison of the Number and Percent of Cloud Layers Retrieved From Radiosonde Data and the WVAP

	Detection scenario 1	Detection scenario 2	Detection scenario 3	Detection scenario 4
Number of cases	160	67	10	11
Percent (in %)	65%	27%	4%	4%

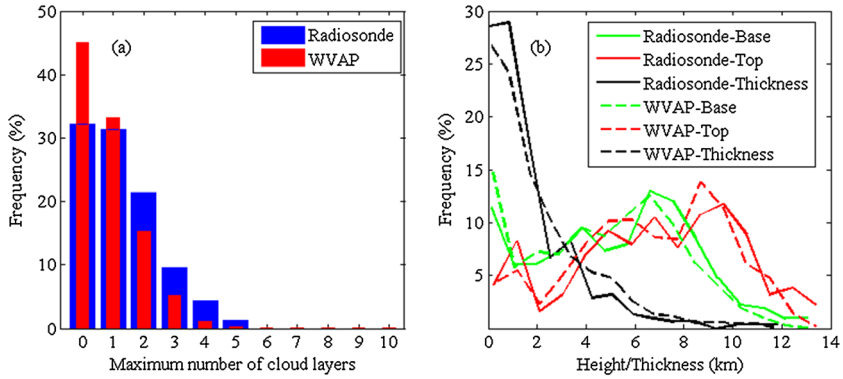

Figure 4. Comparison of cloud layers derived from radiosonde data and the WVAP at the AMF-China site. (a) Frequency distributions of the maximum number of cloud layers, (b) frequency distributions of cloud-base height, cloud-top height, and thickness.

RH which were classified as cloud by the radiosonde but not by the WVAP. Outlier data below the 1:1 line and above 8 km along the *x* axis correspond to a few high-altitude layers classified as cloud by the radiosonde but not by the WVAP. The radiosonde drift is generally larger than 30 km when these layers are detected by the radiosonde. Figures 5c and 5d illustrate the histograms of the differences for cloud-base and cloud-top heights, respectively. Overall, absolute differences are less than 500 m in cloud-base heights and cloud-top heights for 83.3% and 80.7% of the cases analyzed. Of these cases, average differences in cloud-base heights and cloud-top heights are 24.1 m and 57.2 m, respectively; the radiosonde tends to detect higher cloud boundaries.

[20] There are a few cases in Figures 5a and 5b where the cloud boundaries derived from radiosonde and WVAP measurements differ greatly. One explanation is the mismatch

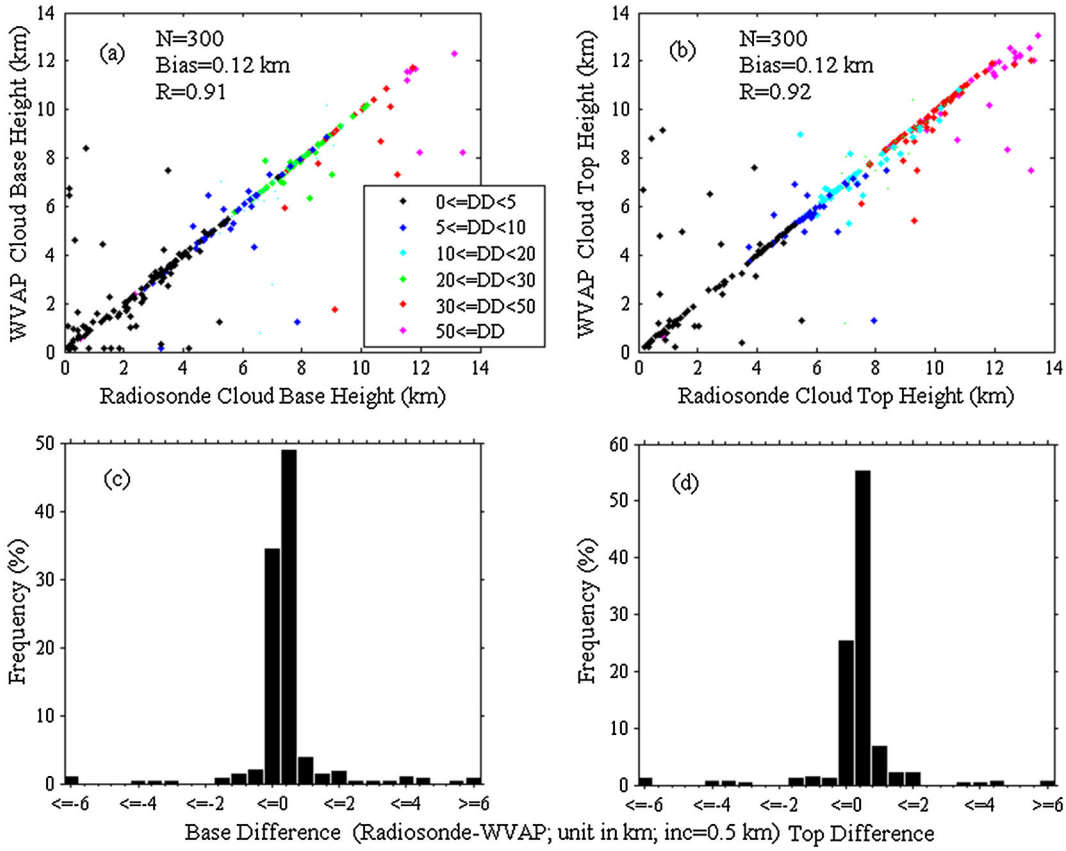

Figure 5. (a) Comparison of cloud-base heights and (b) cloud-top heights derived from radiosonde data and the WVAP at the AMF-China site. Colored dots in Figures 5a and 5b represent different radiosonde drift distances (DD; unit: km). Frequency distributions of (c) cloud-base height differences and (d) cloud-top height differences.

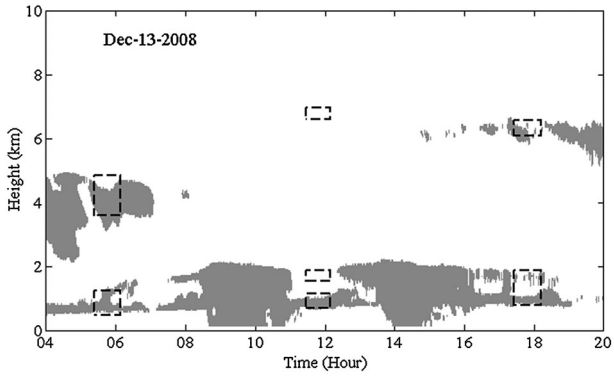

Figure 6. Comparison of cloud layers derived from radiosonde data and the WVAP on 13 December 2008. The areas colored in gray denote the cloud mask from the WVAP; the rectangles outlined in black dashes denote cloud boundaries obtained from three radiosonde launches.

that can occur due to the different detecting perspectives of a fixed ground-based set of instruments and a drifting balloon. As an example, Figure 6 illustrates how the presence of scattered cumulus clouds can lead to differences in detection by the radiosonde and WVAP methods. A continuous time series of the WVAP cloud mask is shown with "snapshots" of cloud layers derived from three radiosonde launches (05:23, 11:27, and 17:25 UTC) superimposed. From this figure and the images taken by a total sky imager camera, we believe this is a convective cloud system. For such clouds, balloon drift can cause a serious misalignment and thus degrade comparison results.

4. Comparisons Between Radiosonde and ARSCL Retrievals at the SGP, TWP, and NSA Sites

[21] Radiosonde types used at the SGP site were the Vaisala RS80-15LH model before May 2001, the RS90-AL model from May 2001 to February 2005, and the RS92-KL model from March 2005 onward. The RH-detecting accuracy of the RS92 radiosonde is about equal to that of the RS90 radiosonde. Although there is a dry bias in RS9x (90 or 92) RH measurements [*Vömel et al.*, 2007; *Miloshevich et al.*, 2009; *Kottayil et al.*, 2012], the detecting accuracy of those radiosondes is higher than that of the RS80 model [*Turner et al.*, 2003; *Miloshevich et al.*, 2006]. The radiosonde-based retrieval method described above was applied to a decade's worth of data from the SGP site (1 January 2001 to 31 December 2010). The mixture of radiosonde models used over this time period results in dry biases of varying magnitude in the data. Unfortunately, correcting the dry bias is complex due to the following three factors: (1) the accuracy of radiosonde RH measurements is not well characterized as a function of height, RH, and solar altitude angle, (2) it differs even for a given radiosonde type owing to hardware, manufacturing, or calibration changes, and (3) the correction of the bias is often obstructed due to a lack of true measurements. The effect of the RS80 dry bias on cloud layer statistics is assumed to be small due to our use of only four months of RS80 data from the SGP site. RS9x

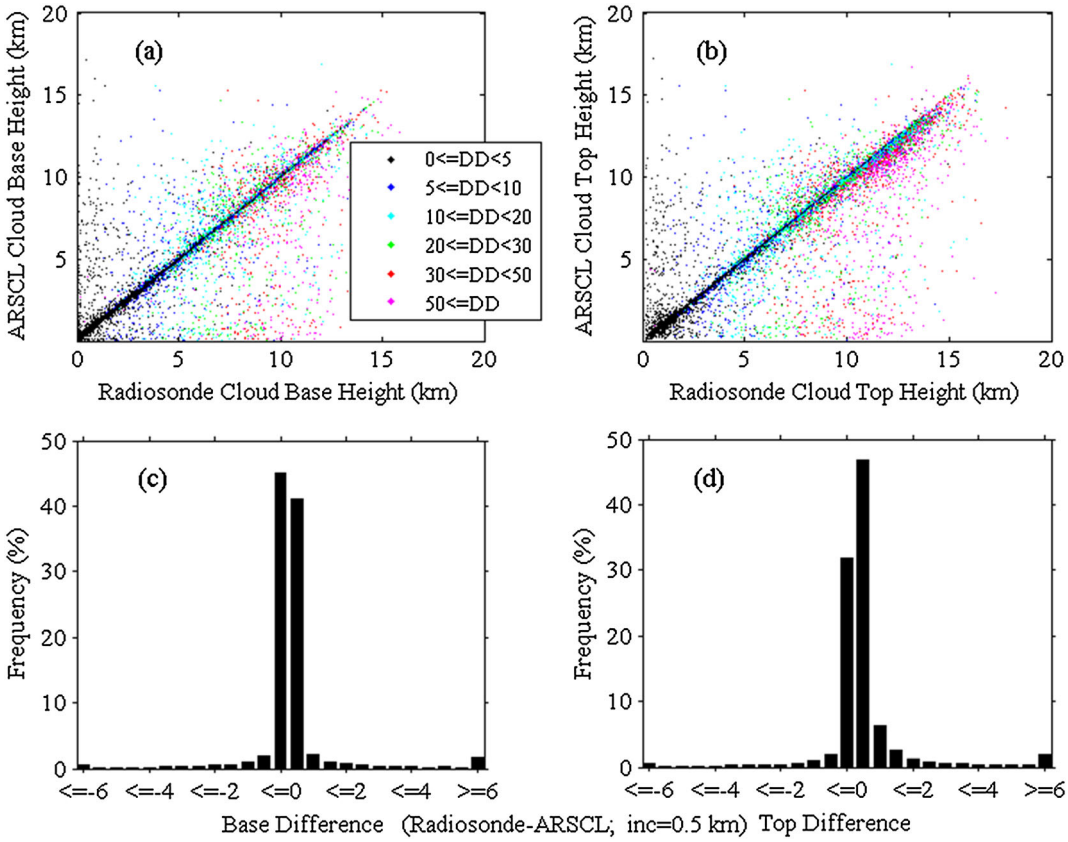

Figure 7. Same as Figure 5 but for the SGP site. Data from a total of 15,701 cloud layers were used in this analysis.

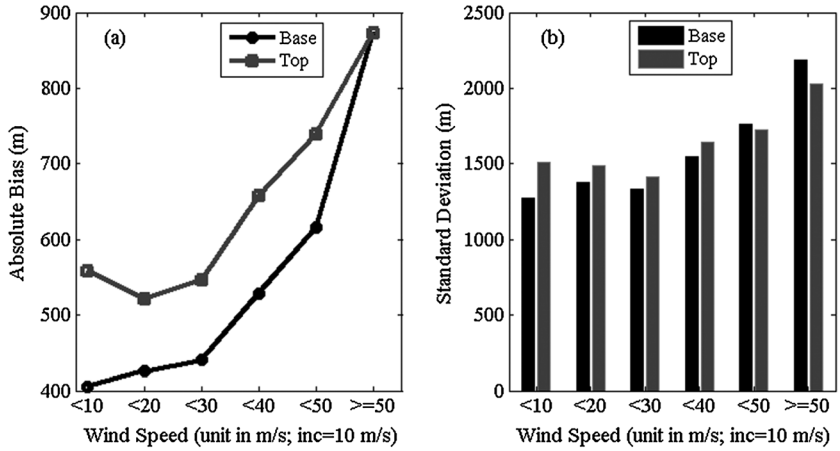

Figure 8. The mean absolute bias (a) and the standard deviation of absolute biases (b) as a function of wind speed at the SGP site. The black (gray) line/bars represent cloud-base (-top) height comparisons using radiosonde and ARSCL retrieval methods.

radiosonde data from June 2002 onward and from April 2002 onward at the TWP and NSA sites, respectively, are used here.

4.1. Comparisons of Cloud Layers Derived at the SGP Site

[22] A total of 15,701 cloud boundaries obtained from radiosonde data and ARSCL retrievals are compared. Figures 7a and 7b show the comparisons for cloud-base and cloud-top heights, respectively. Overall, the retrievals of both cloud boundaries agree very well. The correlation coefficient, mean bias, mean absolute bias, root mean square, and standard deviation for the cloud-base height comparison are 0.92, 0.11 km, 0.46 km, 1.49 km, and 1.49 km, respectively. For cloud-top heights, they are 0.92, 0.26 km, 0.60 km, 1.69 km, and 1.67 km, respectively. An overwhelmingly large number of data points fall along or overlap the 1:1 line. Outlier points result from the same factors described previously:

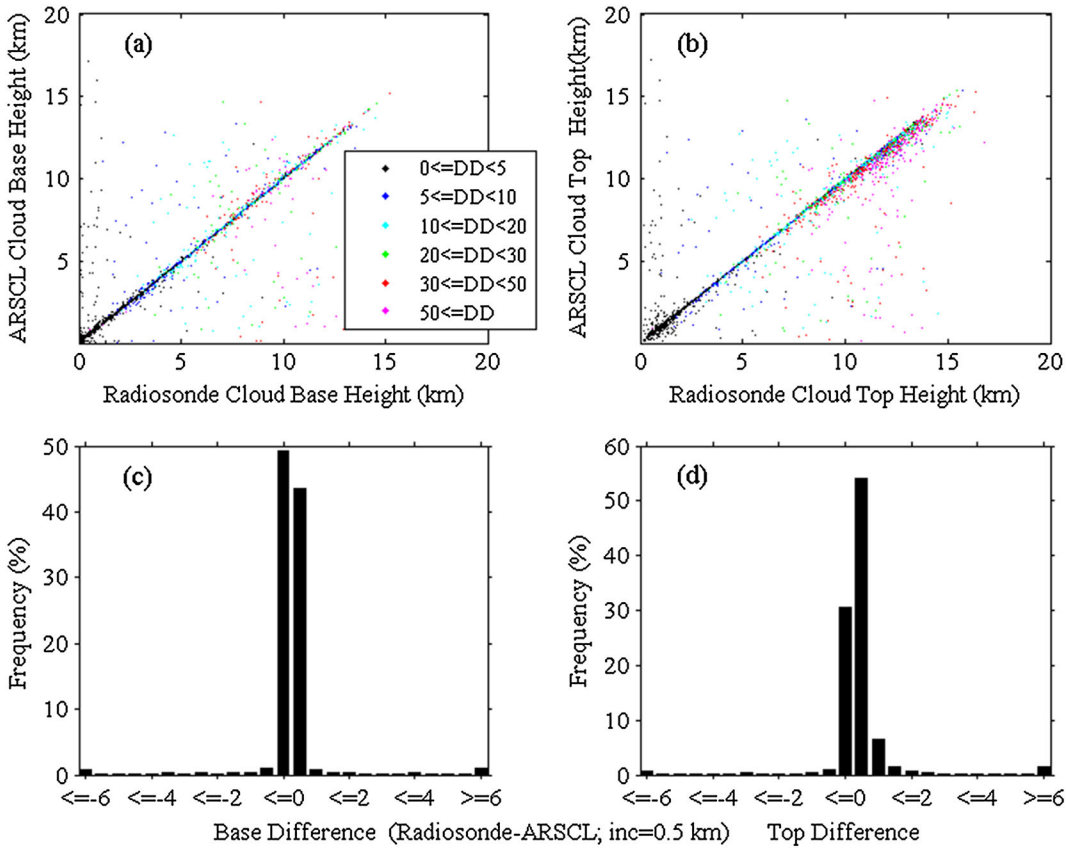

Figure 9. Same as Figure 7 but for single-layer clouds. Data from a total of 3761 cloud layers were used in this analysis.

inhomogeneous cloud and balloon drift. Figures 7c and 7d show histograms of their cloud-base and cloud-top height differences. For 86.1% (78.7%) of clouds detected by both methods, their base (top) heights differ by less than 500 m. Of these cases, average differences in cloud-base heights and cloud-top heights are -4.3 m and 41.6 m, respectively; the radiosonde tends to detect higher cloud-top heights.

[23] As mentioned earlier, a major problem is the mismatch between radiosonde- and ground-based observations due to balloon drift. The agreement between the two cloud boundary retrieval methods is investigated as a function of wind, which is measured by the radiosonde and interpolated to radiosonde-derived cloud boundary levels. Figure 8a shows mean absolute biases for cloud-base and -top height retrievals as a function of wind speed, and Figure 8b shows how the standard deviation of absolute biases changes with wind speed. In general, both the mean absolute bias and the standard deviation increase with increasing wind speed. The large wind speeds result in great balloon drifts and fast cloud layer movement and can thus cause the mismatch between cloud retrievals from the two approaches.

[24] Figure 9 shows the same comparison but for single-layer clouds only. The mean bias for cloud-base heights and cloud-top heights are -2.5 m and 171.8 m, respectively. Absolute differences are less than 500 m in cloud-base (cloud-top) heights for 92.6% (84.5%) of the cases analyzed. The agreement between the two cloud retrieval methods is much better for single-layer clouds than for all other cloud layer configurations considered here. This is due to how the accuracy of radiosonde observations is affected after the balloon travels through a cloud layer. There is often a delay (time lag) after the radiosonde passes through a cloud layer because of the wetness of the sensors. This also explains why (1) radiosonde-retrieved cloud bases are more accurate than cloud-top retrievals, and (2) the radiosonde tends to detect higher cloud-top heights than that retrieved from the ARSCL.

4.2. Comparisons of Cloud Layers Derived at the TWP Site

[25] The same analysis is conducted on data collected at the TWP site. A total of 9283 cloud boundaries derived from radiosonde data and ARSCL retrievals are compared and results are presented in Figure 10. Overall, the agreement between retrievals of both cloud-base and cloud-top heights is reasonable. The correlation coefficient, mean bias, mean absolute bias, root mean square, and standard deviation for the cloud-base height comparison are 0.94, 0.05 km, 0.63 km, 1.63 km, and 1.63 km, respectively. For cloud-top heights, they are 0.92, 0.38 km, 0.94 km, 2.13 km, and 2.10 km, respectively. Again, an overwhelmingly large number of data points fall along or overlap the 1:1 line. Figures 10c and 10d show histograms of their cloud-base and cloud-top differences. For 77.1% (66.7%) of clouds detected by both methods, their base (top) heights differ by less than 500 m. Of these cases, average differences in cloud-base heights

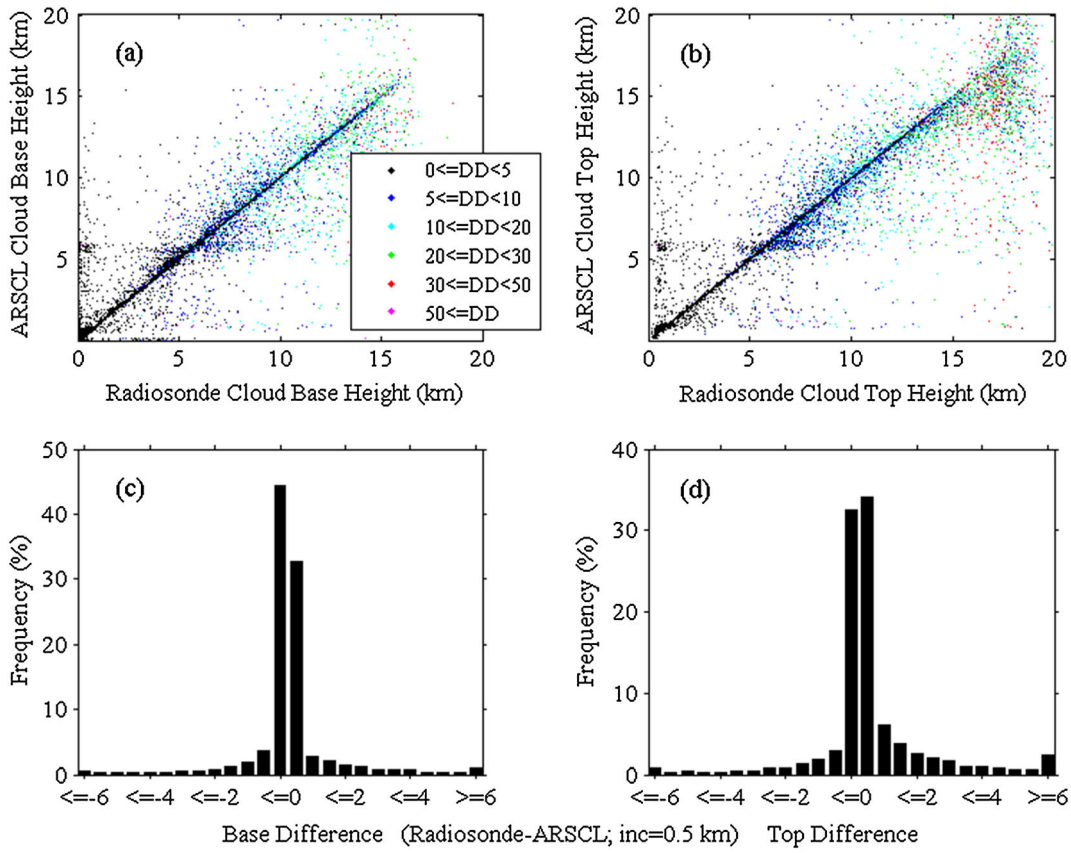

Figure 10. Same as Figure 7 but for the TWP site. Data from a total of 9283 cloud layers were used in this analysis.

and cloud-top heights are -28.2 m and 10.4 m, respectively; the radiosonde tends to detect higher cloud-top heights. Absolute differences are less than 500 m in cloud-base (cloud-top) heights for 81.5% (70.0%) of single-layer cloud cases (not shown here).The agreement between cloud layers derived from radiosonde data and ARSCL at the TWP site is not as good as the agreement found in data from the SGP site.

4.3. Comparisons of Cloud Layers Derived at the NSA Site

[26] A total of 9224 cloud boundaries derived from radiosonde data and ARSCL retrievals are compared and results are presented in Figure 11. Figures 11a and 11b show the comparisons for cloud-base and cloud-top heights, respectively. The correlation coefficient, mean bias, mean absolute bias, root mean square, and standard deviation for the cloud-base height comparison are 0.80, 0.50 km, 0.87 km, 2.05 km, and 2.00 km, respectively. For cloud-top heights, they are 0.80, 0.75 km, 1.14 km, 2.34 km, and 2.21 km, respectively. Figures 11c and 11d present the histograms of their differences for cloud-base and cloud-top heights. For 73.1% (61.2%) of clouds detected by both methods, their base (top) heights differ by less than 500 m. Of these cases, average differences in cloud-base heights and cloud-top heights are 28.6 m and 56.8 m, respectively; the radiosonde tends to detect higher cloud boundaries. The same comparisons are also made for single-layer cloud cases (not shown here). Absolute differences are less than 500 m in cloud-base (cloud-top) heights for 90.6% (70.0%) of the cases analyzed.

[27] Similar to the situation at the TWP site, more high altitude cloud layers are detected by the radiosonde, as illustrated by the outlier points below the 1:1 line in Figures 11a and 11b. An example is given in Figure 12 to illustrate how this arises. In Figure 12a, profiles of RH are shown with respect to water and ice for a radiosonde launch on 24 January 2006 at 21:35 UTC. Gray areas represent radiosonde-derived cloud layer boundaries. Figure 12b shows the ARSCL cloud mask generated during the radiosonde launch period. The bottommost four radiosonde-derived cloud layers agree very well with ARSCL retrievals. However, the uppermost cloud layer detected by the radiosonde was classified as a clear layer of air in the ARSCL retrieval. Note that RH values with respect to ice are over the saturation point at most levels within radiosonde-based cloud layers. A closer look at all cloud layer retrievals from the two methods reveals that this situation occurs quite frequently. Further studies are needed to investigate the relationship between cloud formations and RH distributions in the upper part of the troposphere at the NSA site.

[28] A summary of radiosonde and ARSCL retrievals of cloud boundaries at the SGP, TWP, and NSA sites is given in Table 2.

5. Conclusions and Discussions

[29] The ARM mobile facility was deployed in Shouxian, China from 14 May to 28 December 2008. During the field

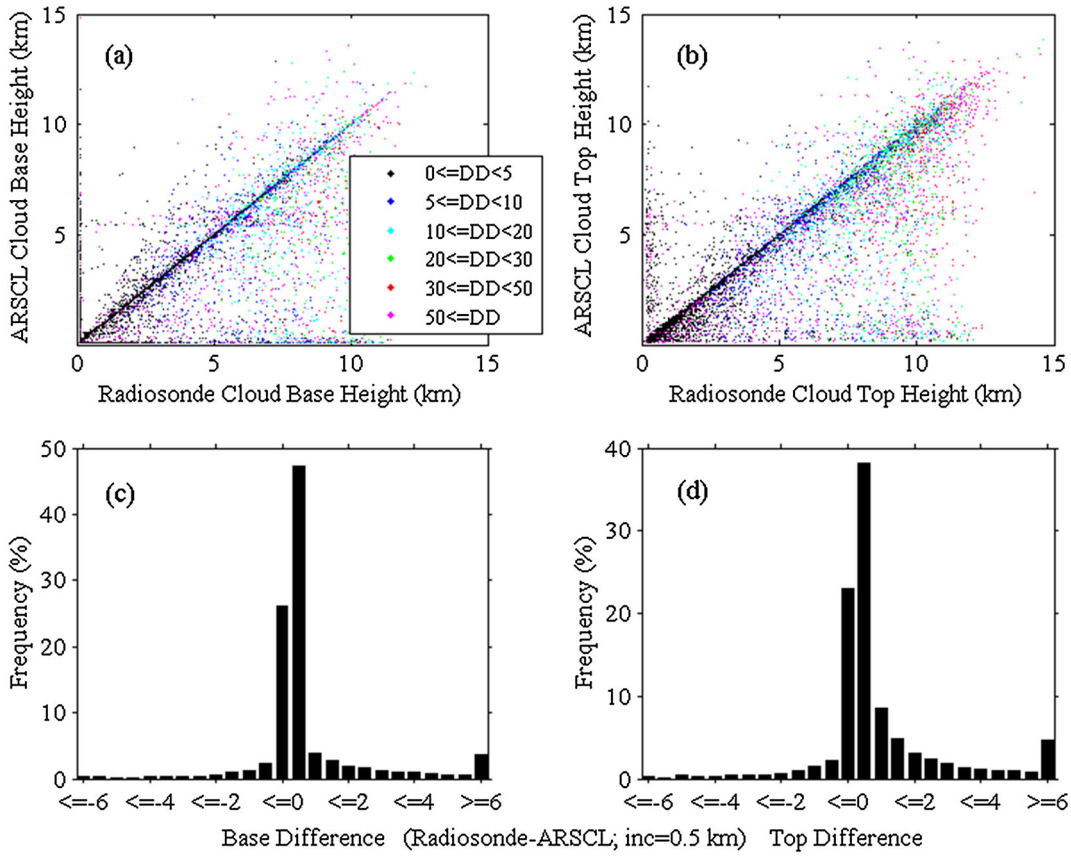

Figure 11. Same as Figure 7 but for the NSA site. Data from a total of 9224 cloud layers were used in this analysis.

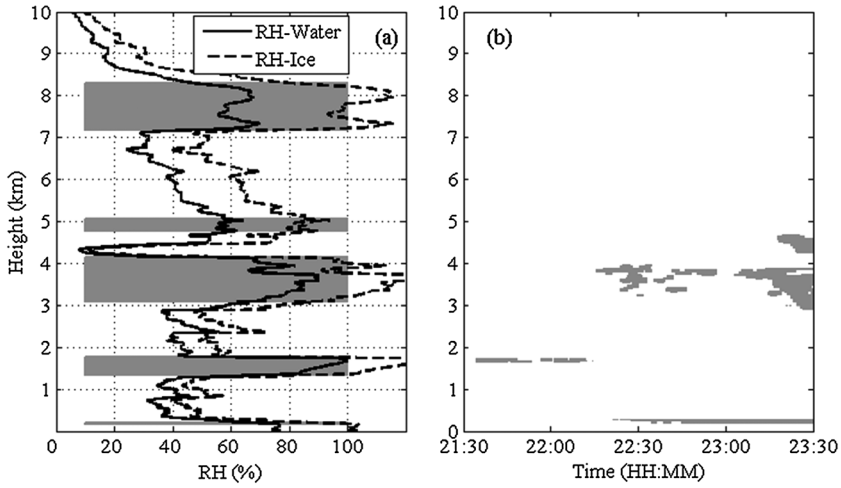

Figure 12. Comparison of cloud layers obtained from radiosonde data (a) and ARSCL retrievals (b). Radiosonde vertical profiles of RH with respect to water, RH with respect to ice when temperatures are less than 0°C, and cloud layer boundaries are shown by the solid black line, the dashed black line, and the area colored cyan, respectively. Cloud layers from ARSCL retrievals in Figure 12b are drawn in cyan.

Table 2. Summary of Radiosonde and ARSCL Retrievals of Cloud Boundaries at the SGP, TWP, and NSA Sites[a]

Sites	Bias	AbsBia	StdDev	R	P_{500}
Cloud Base Heights					
SGP	0.11	0.46	1.49	0.92	86.1%
TWP	0.05	0.63	1.63	0.94	77.1%
NSA	0.50	0.87	2.00	0.80	73.1%
Cloud Top Heights					
SGP	0.26	0.60	1.67	0.92	78.7%
TWP	0.38	0.94	2.10	0.92	66.7%
NSA	0.75	1.14	2.21	0.80	61.2%

[a]Included are the mean bias (unit in km), the mean absolute bias (AbsBia; unit in km), the standard deviation (StdDev; units in km), the correlation coefficient (R), and the percentage of clouds where boundary heights from both methods differed by less than 500 m (P_{500}).

campaign, radiosondes were launched four times a day without any major interruption. The 95-GHz WACR was also deployed at the site from 15 October to 15 December 2008. Radiosonde-based cloud layers were compared to those retrieved from the WACR-ARSCL ground-based remote sensing product generated during the field campaign. Many layers near the surface were classified as cloud layers by the WACR-ARSCL. Absolute differences in cloud-base heights and cloud-top heights from radiosonde and WACR-ARSCL retrievals are less than 500 m for 83.3% and 80.7% of the cases analyzed, respectively. Large differences between cloud boundaries from the two retrieval methods are mainly due to balloon drift.

[30] To test how the radiosonde-based cloud retrieval method performs using data from different geographic locations and climate regimes, the method was applied to a decade's worth of radiosonde data collected at the SGP Central Facility, the TWP Manus Facility, and the Barrow, Alaska Facility and comparisons to ground-based remote sensing retrievals were made. Overall, cloud layers derived from the two approaches agree very well at the SGP site. Absolute differences in cloud-base heights and cloud-top heights from radiosonde and millimeter cloud radar retrievals are less than 500 m for 86.1% and 78.7% of the cases analyzed, respectively; for single-layer cloud cases, absolute differences are 92.6% and 84.5%, respectively. The agreement between the two cloud retrieval methods is best for single-layer clouds than for any other cloud configuration.

[31] The radiosonde-based cloud retrieval method was originally developed using data collected at the AMF-China site. Both AMF-China and SGP sites are located in the midlatitudes and have similar climates so it is not surprising that radiosonde and ground-based remote sensing retrievals of cloud layers at these two locations agree very well. Greater differences are seen at the TWP and NSA sites, which represent different climate regimes. The radiosonde tends to detect more cloud layers in the upper troposphere than does the ARSCL product. The TWP Manus site, located in the core of the Pacific oceanic warm pool, consistently has the warmest sea-surface temperature. This warm body of water supplies heat and moisture to the atmosphere above it, causing the formation of deep convective cloud systems and cirrus clouds located at high altitude. The NSA Barrow site offers a cold contrast. Ice is the predominant form of condensed water in the air for most of the year, and there is very little water vapor in the atmosphere. Cloud formation changes with climate regime so the radiosonde-based cloud layer retrieval method developed using data from one location may not be applicable to data from another location with a different climate regime. To improve the performance of the radiosonde-based cloud layer retrieval method and its adaptation to different climate regimes, further studies are needed to investigate the relationship between cloud formations and RH distributions in the Tropics and at high latitude regions, and especially in the upper parts of the atmosphere.

[32] **Acknowledgments.** The data used in this study were made available by the Atmospheric Radiation Measurement (ARM) Program sponsored by the U.S. Department of Energy (DOE). We would like to thank all participants in the ARM experiment. This work is supported by the Ministry of Science and Technology of China (2010CB950804, 2013CB955804), the National Natural Science Foundation of China (40830102), DOE (DESC0007171) and National Science Foundation (AGS-1118325).

References

Arabey, E. N. (1975), Radiosounding data as means for cloud layers revealing cloud layer (in Russian), *Meteorol. Gidrol.*, *6*, 23–37.

Air Weather Service (1979), The use of the skew of T, log P diagram in analysis and forecasting, *Tech. Rep. AWS/TR-79/006*, 150 pp., Scott AFB, Ill.

Chang, F.-L., and Z. Li (2005a), A new method for detection of cirrus overlapping water clouds and determination of their optical properties, *J. Atmos. Sci.*, *62*, 3993–4009.

Chang, F.-L., and Z. Li (2005b), A comparison of the global surveys of high, mid, and low clouds from satellites and general circulation models, in *Fifteenth ARM Science Team Meeting Proceedings*, Daytona Beach, Fla, Atmospheric Radiation Measurement Program, US Department of Energy.

Chahine, M. T., et al. (2006), AIRS improving weather forecasting and providing new data on greenhouse gases, *Bull. Am. Meteorol. Soc.*, *87*, 911–926.

Chernykh, I. V., and R. E. Eskridge (1996), Determination of cloud amount and level from radiosonde soundings, *J. Appl. Meteorol.*, *35*, 1362–1369.

Chernykh, I. V., O. A. Alduchov, and R. E. Eskridge (2000), Trends in low and high cloud boundaries and errors in height determination of cloud boundaries, *Bull. Am. Meteorol. Soc.*, *82*(9), 1941–1947.

Clothiaux, E. E., et al. (1999), The Atmospheric Radiation Measurement Program cloud radars: operational modes, *J. Atmos. Oceanic Technol.*, *16*, 819–827, doi:10.1175/1520-0426(1999)016 < 0819:TARMPC > 2.0.CO;2.

Clothiaux, E. E., T. P. Ackerman, G. C. Mace, K. P. Moran, R. T. Marchand, M. A. Miller and B. E. Martner (2000), Objective determination of cloud heights and radar reflectivities using a combination of active remote sensors at the ARM CART sites, *J. Appl. Meteorol.*, *39*, 645–665.

Dolgin, M. I. (1983), Determine scheme clouds from atmosphere sounding in Antarctic Continent (in Russian), *Meterol. Gidrol.*, *11*, 47–51.

Dong, X., and G. G. Mace (2003), Arctic stratus cloud properties and radiative forcing derived from ground-based data collected near Point Barrow, Alaska, *J. Clim.*, *16*, 445–461.

Dong, X., P. Minnis, and B. Xi (2005), A climatology of midlatitude continental clouds from the ARM SGP central facility: Part I: Low-level cloud macrophysical, microphysical, and radiative properties, *J. Clim.*, *18*, 1391–1410.

Dong, X., B. Xi, and P. Minnis (2006), A climatology of midlatitude continental clouds from the ARM SGP central facility. Part II: Cloud fraction and surface radiative forcing, *J. Clim.*, *19*, 1765–1783.

Fan, J., T. Yuan, J. M. Comstock, S. Ghan, A. Khain, L. R. Leung, Z. Li, V. J. Martins, and M. Ovchinnikov (2009), Dominant role by vertical wind shear in regulating aerosol effects on deep convective clouds, *J. Geophys. Res.*, *114*, D22206, doi:10.1029/2009JD012352.

Fan, J., D. Rosenfeld, Y. Ding, R. Leung, and Z. Li (2012), Potential aerosol indirect effects on atmospheric circulation and radiative forcing through deep convection, *Geophys. Res. Lett.*, *39*, L09806, doi:10.1029/2012GL051851.

Haeffelin, M., et al. (2005), SIRTA, a ground-based atmospheric observatory for cloud and aerosol research, *Ann. Geophys.*, *23*, 253–275.

Illingworth, A. J., et al. (2007), Cloudnet—Continuous evaluation of cloud profiles in seven operational models using ground-based observations, *Bull. Am. Meteorol. Soc.*, *88*, 883–898, doi:qj.00010.1175/BAMS-88-6-883.

Jakob, C., G. Tselioudis, and T. Hume (2005), The radiative, cloud, and thermodynamic properties of the major tropical western Pacific cloud regimes, *J. Clim.*, *18*, 1203–1215, doi:10.1175/JCLI3326.1.

Kollias, P., G. Tselioudis, and B. A. Albrecht (2007), Cloud climatology at the Southern Great Plains and the layer structure, drizzle, and atmospheric modes of continental stratus, *J. Geophys. Res.*, *112*, D09116, doi:10.1029/2006JD007307.

Kollias, P., M. A. Miller, K. L. Johnson, M. P. Jensen, and D. T. Troyan (2009), Cloud, thermodynamic, and precipitation observations in West Africa during 2006, *J. Geophys. Res.*, *114*, D00E08, doi:10.1029/2008JD010641.

Kottayil, A., S. Buehler, V. John, L. Miloshevich, M. Milz, and G. Holl (2012), On the importance of Vaisala RS92 radiosonde humidity corrections for a better agreement between measured and modeled satellite radiances, *J. Atmos. Oceanic Technol.*, *29*(2), 248–259, doi:10.1175/JTECH-D-11-00080.1.

Lazarus, S. M., S. K. Krueger, and G. G. Mace (2000), A cloud climatology of the Southern Great Plains ARM CART, *J. Clim.*, *13*, 1762–1775.

Li, Z., M. C. Cribb, F.-L. Chang, A. Trishchenko, and Y. Luo (2005), Natural variability and sampling errors in solar radiation measurements for model validation over the Atmospheric Radiation Measurement Southern Great Plains region, *J. Geophys. Res.*, *110*, D15S19, doi:10.1029/2004JD005028.

Li, Z., K. H. Lee, Y. Wang, J. Xin, and W. M. Hao (2010), First observation-based estimates of cloud free aerosol radiative forcing across China, *J. Geophys. Res.*, *115*, D00K18, doi:10.1029/2009JD013306.

Li, Z., et al. (2011a), East Asian studies of tropospheric aerosols and their impact on regional climate (EASTAIRC): An overview, *J. Geophys. Res.*, *116*, D00K34, doi:10.1029/2010JD015257.

Li, Z., F. Niu, J. Fan, Y. Liu, D. Rosenfeld, and Y. Ding (2011b), Long-term impacts of aerosols on the vertical development of clouds and precipitation, *Nat. Geosci.*, *4*, 888–894, doi:10.1038/ngeo1313.

Mace, G. G., and S. Benson (2008), The vertical structure of cloud occurrence and radiative forcing at the SGP ARM site as revealed by 8 years of continuous data, *J. Clim.*, *21*(11), 2591, doi:10.1175/2007JCLI1987.1.

Mace, G. G., Q. Zhang, M. Vaughan, R. Marchand, G. Stephens, C. Trepte, and D. Winker, (2009), A description of hydrometeor layer occurrence statistics derived from the first year of merged Cloudsat and CALIPSO data, *J. Geophys. Res.*, *114*, D00A26, doi:10.1029/2007JD009755.

Marchand, R. T., T. P. Ackerman, and C. Moroney (2007), An assessment of Multiangle Imaging Spectroradiometer (MISR) stereo-derived cloud top heights and cloud top winds using ground-based radar, lidar, and microwave radiometers, *J. Geophys. Res.*, *112*, D06204, doi:10.1029/2006JD007091.

Mather, J. H., S. A. McFarlane, M. A. Miller, and K. L. Johnson (2007), Cloud properties and associated radiative heating rates in the tropical western Pacific, *J. Geophys. Res.*, *112*, D05201, doi:10.1029/2006JD007555.

Miller, M. A., K. L. Johnson, D. T. Troyan, E. E. Clothiaux, E. J. Mlawer, and G. G. Mace (2003), ARM value-added cloud products: Description and status, in *Proceedings of the 13th ARM Science Team Meeting*, 31 March to 4 April 2003, Broomfield, Colo. [Available at http://www.arm.gov/publications/proceedings/conf13/extended_abs/miller-ma.pdf.]

Miller, M. A. (2008), The Cloud and Land Surface Interaction Campaign (CLASIC), *Eos Trans. AGU*, *89*(23), Jt. Assem. Suppl., Abstract H43D-03.

Miloshevich, L. M., H. Vömel, D. N. Whiteman, B. M. Lesht, F. J. Schmidlin, and F. Russo (2006), Absolute accuracy of water vapor measurements from six operational radiosonde types launched during AWEX-G and implications for AIRS validation, *J. Geophys. Res.*, *111*, D09S10, doi:10.1029/2005JD006083.

Miloshevich, L. M., H. Vömel, D. N. Whiteman, and T. Leblanc (2009), Accuracy assessment and correction of Vaisala RS92 radiosonde water vapor measurements, *J. Geophys. Res.*, *114*, D11305, doi:10.1029/2008JD011565.

Minnis, P., Y. Yi, J. Huang, and J. K. Ayers (2005), Relationships between radiosonde and RUC-2 meteorological conditions and cloud occurrence determined from ARM data, *J. Geophys. Res.*, *110*, D23204, doi:10.1029/2005JD006005.

Moran, K. P., B. E. Martner, M. J. Post, R. A. Kropfli, D. C. Welsh, and K. B. Widener (1998), An unattended cloud-profiling radar for use in climate research, *Bull. Am. Meteorol. Soc.*, *79*, 443–455.

Naud, C., J.-P. Muller, and E. E. Clothiaux (2003), Comparison between active sensor and radiosonde cloud boundaries over the ARM Southern Great Plains site, *J. Geophys. Res.*, *108*(D4), 4140, doi:10.1029/2002JD002887.

Niu, F., and Z. Li, (2012), Systematic variations of cloud top temperature and precipitation rate with aerosols over the global tropics, *Atmos. Chem. Phys.*, *12*, 8491–8498, doi:10.5194/acp-12-8491-2012.

Nowak, D., D. Rueux, J. L. Agnew, and L. Vuilleumier (2008), Detection of fog and low cloud boundaries with ground-based remote sensing systems, *J. Atmos. Ocean. Technol.*, *25*, 1357–1368.

Oreopoulos, L., and P. M. Norris, (2011), An analysis of cloud overlap at a midlatitude atmospheric observation facility, *Atmos. Chem. Phys., Disc.*, *11*, 597–625.

Pavolonis, M. J., A. K. Heidinger, and T. Uttal (2005), Daytime global cloud typing from AVHRR and VIIRS: Algorithm description, validation, and comparisons, *J. Appl. Meteorol.*, *44*, 804–826, doi:10.1175/JAM2236.1.

Poore, K. D., J. Wang, and W. Rossow (1995), Cloud layer thickness from a combination of surface and upper-air observations, *J. Clim.*, *8*, 550–568.

Qian Y., C. Long, H. Wang, J. Comstock, S. McFarlane, and S. Xie (2012), Evaluation of cloud fraction and its radiative effect simulated by IPCC AR4 global models against ARM surface observations, *Atmos. Chem. Phys.*, *12*(4), 1785–1810, doi:10.5194/acp-12-1785-2012.

Stephens, G. L., et al. (2002), The CloudSat mission and the A-TRAIN: A new dimension to space-based observations of clouds and precipitation, *Bull. Am. Meteorol. Soc.*, *83*, 1771–1790.

Tobin, D. C., H. E. Revercomb, R. O. Knuteson, B. M. Lesht, L. L. Strow, S. E. Hannon, W. F. Feltz, L. A. Moy, E. J. Fetzer, and T. S. Cress (2006), Atmospheric Radiation Measurement site atmospheric state best estimates for Atmospheric Infrared Sounder temperature and water vapor retrieval validation, *J. Geophys. Res.*, *111*, D09S14, doi:10.1029/2005JD006103.

Turner, D. D., B. M. Lesht, S. A. Clough, J. C. Liljegren, H. E. Revercomb, and D. C. Tobin (2003), Dry bias and variability in Vaisala RS80-H radiosondes: The ARM experience, *J. Atmos. Oceanic Technol.*, *20*, 117–132.

Vömel, H., et al. (2007), Radiation dry bias of the Vaisala RS92 humidity sensor, *J. Atmos. Oceanic Technol.*, *24*, 953–963.

Wang, J., and W. B. Rossow (1995), Determination of cloud vertical structure from upper air observations, *J. Appl. Meteorol.*, *34*, 2243–2258.

Wang, J., W. B. Rossow, T. Uttal, and M. Rozendaal (1999), Variability of cloud vertical structure during ASTEX observed from a combination of rawinsonde, radar, ceilometer, and satellite, *Mon. Weather Rev.*, *127*, 2482–2502.

Wang, J., W. B. Rossow, and Y. Zhang (2000), Cloud vertical structure and its variations from a 20-year global rawinsonde dataset, *J. Clim.*, *13*, 3041–3056.

Xi, B., X. Dong, P. Minnis, and M. M. Khaiyer (2010), A 10-year climatology of cloud cover and vertical distribution derived from both surface and GOES observations over the DOE ARM SGP Site, *J. Geophys. Res.*, *115*, D12124, doi:10.1029/2009JD012800.

Xie, S., S. A. Klein, J. J. Yio, A. C. M. Beljaars, C. N. Long, and M. Zhang (2006), An assessment of ECMWF analyses and model forecasts over the North Slope of Alaska using observations from the ARM Mixed-Phase Arctic Cloud Experiment, *J. Geophys. Res.*, *111*, D05107, doi:10.1029/2005JD006509.

Zhang, J., H. Chen, Z. Li, X. Fan, L. Peng, Y. Yu, and M. Cribb (2010), Analysis of cloud layer structure in Shouxian, China using RS92 radiosonde aided by 95 GHz cloud radar, *J. Geophys. Res.*, *115*, D00K30, doi:10.1029/2010JD014030.

Zhang, Y., and S. A. Klein (2010), Mechanisms affecting the transition from shallow to deep convection over land: Inferences from observations of the diurnal cycle collected at the ARM southern great plains site, *J. Atmos. Sci.*, *67*, 2943–2959.

Zhao, M., and Z. Wang (2010), Comparison of Arctic clouds between European Center for Medium-Range Weather Forecasts simulations and Atmospheric Radiation Measurement Climate Research Facility long-term observations at the North Slope of Alaska Barrow site, *J. Geophys. Res.*, *115*, D23202, doi:10.1029/2010JD014285.